

## VELOCITY DISPERSION PROFILE OF THE MILKY WAY HALO

WARREN R. BROWN, MARGARET J. GELLER, SCOTT J. KENYON  
Smithsonian Astrophysical Observatory, 60 Garden St, Cambridge, MA 02138, USA

ANTONALDO DIAFERIO

Dipartimento di Fisica Generale ‘Amedeo Avogadro’, Università degli Studi di Torino, Via P. Giuria 1, I-10125 Torino, Italy and  
Istituto Nazionale di Fisica Nucleare (INFN), Sezione di Torino, Via P. Giuria 1, I-10125, Torino, Italy

*Draft version October 22, 2018*

### ABSTRACT

We present a spectroscopic sample of 910 distant halo stars from the Hypervelocity Star survey from which we derive the velocity dispersion profile of the Milky Way halo. The sample is a mix of 74% evolved horizontal branch stars and 26% blue stragglers. We estimate distances to the stars using observed colors, metallicities, and stellar evolution tracks. Our sample contains twice as many objects with  $R > 50$  kpc as previous surveys. We compute the velocity dispersion profile in two ways: with a parametric method based on a Milky Way potential model, and with a non-parametric method based on the caustic technique originally developed to measure galaxy cluster mass profiles. The resulting velocity dispersion profiles are remarkably consistent with those found by two independent surveys based on other stellar populations: the Milky Way halo exhibits a mean decline in radial velocity dispersion of  $-0.38 \pm 0.12$  km s<sup>-1</sup> kpc<sup>-1</sup> over  $15 < R < 75$  kpc. This measurement is a useful basis for calculating the total mass and mass distribution of the Milky Way halo.

*Subject headings:* Galaxy: halo — Galaxy: kinematics and dynamics —

### 1. INTRODUCTION

A fundamental property of the Milky Way galaxy is its total mass. In the Cold Dark Matter paradigm, the total mass of a galaxy’s dark matter halo correlates with its merger history, star formation history, and number of its satellite sub-halos. A galaxy’s mass distribution is also a fundamental constraint on theories. Cold dark matter models predict that density follows an universal NFW profile (Navarro et al. 1997); in Modified Newtonian Dynamics there is no dark matter halo and the mass distribution is highly flattened compared to cold dark matter models (Hernandez et al. 2009). The Milky Way provides an unique laboratory for testing these issues.

Nevertheless, the mass and mass distribution of the Milky Way are among the most poorly known of all Galactic parameters, especially at large distances  $R \gtrsim 50$  kpc. Total mass estimates span at least a factor of 4, from  $0.5 \times 10^{12}$  to  $2 \times 10^{12}$  M<sub>⊙</sub> (see below). Recent theoretical work based on semi-analytic models and timing arguments suggest the Milky Way may be even more massive (Li & White 2008; Abadi et al. 2009). Clearly, the mass and mass distribution of the Milky Way remain controversial and important issues.

A powerful approach for measuring the Milky Way’s mass distribution is measuring the motions of tracer objects. Radio masers probe the Galactic rotation curve out to 15 kpc (Reid et al. 2009); H I gas probes the rotation curve to larger distances (Kalberla & Dedes 2008). Luminous tracers at  $R \gtrsim 50$  kpc, however, are rare. Historically, globular clusters and dwarf galaxies were used to measure the total mass of the Milky Way (e.g. Little & Tremaine 1987; Zaritsky et al. 1989; Kulessa & Lynden-Bell 1992; Kochanek 1996; Wilkinson & Evans 1999). These mass estimates were

based on samples of a few dozen objects, and suffered from a systematic factor of  $\sim 2$  uncertainty depending on the inclusion of Leo I. Post-main sequence halo stars provide denser tracers, but the blue horizontal branch (BHB) star samples of Sommer-Larsen et al. (1997) and Sakamoto et al. (2003) are limited to  $R \lesssim 20$  kpc. Battaglia et al. (2005) added 58 distant red giants from the Spaghetti survey and claimed a large decline in the velocity dispersion at  $R > 50$  kpc. Recently, Xue et al. (2008) analyzed the Sloan Digital Sky Survey (SDSS) sample of 2,466 BHB stars and found a small decline in velocity dispersion with distance. Only 80 of the SDSS BHB stars are located at  $R > 50$  kpc.

Here we use the distant halo stars from the hypervelocity star (HVS) program (Brown et al. 2005a, 2006a,b, 2007b,c, 2009a,b) to measure the velocity dispersion profile of the Milky Way. Our dataset is a complete spectroscopic sample of 910 stars observed over 7300 deg<sup>2</sup> of the SDSS Data Release 6 imaging region. We gain increased leverage on the velocity dispersion profile for  $R \gtrsim 50$  kpc. We find an average decline in radial velocity dispersion of  $0.38 \pm 0.12$  km s<sup>-1</sup> kpc<sup>-1</sup> over  $15 < R < 75$  kpc.

In §2 we describe the observations and luminosity estimates for stars in our sample. In §3 we make parametric and non-parametric estimates of the velocity dispersion profile. We also discuss possible systematics, and compare our results with earlier work. We conclude in §4. The data are in the Appendix.

### 2. DATA

The hypervelocity star program is a radial velocity survey of stars selected with the colors of late B-type stars. The radial velocity survey is now 93% complete over 7300 deg<sup>2</sup> of the SDSS DR6 imaging footprint. Here we focus exclusively on the stars with late-B and early-A spectral types; we exclude all white dwarfs (Kilic et al. 2007a,b),

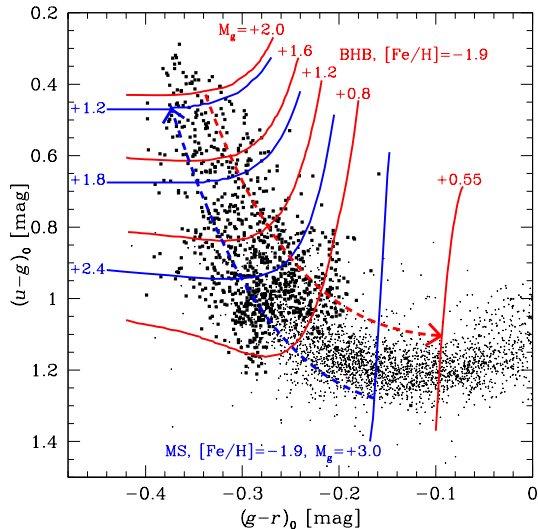


FIG. 1.— Color-color diagram showing the distribution of the HVS survey stars (*solid squares*) and the Xue et al. (2008) BHB stars (*dots*) compared to lines of constant absolute magnitude  $M_g$  for BHB stars (red lines, Dotter et al. 2008) and main sequence stars (blue lines Girardi et al. 2004). All tracks are for  $[\text{Fe}/\text{H}]=-1.9$ , the mean metallicity of halo stars. Dashed lines indicate the direction of increasing luminosity. At  $[\text{Fe}/\text{H}]=-1.9$ , BHB stars and blue stragglers share identical luminosities around  $(u-g)_0 \simeq 0.6$ .

B supergiants (Brown et al. 2007a), emission line galaxies (Kewley et al. 2007; Brown et al. 2008b), and quasars (Brown et al. 2009a).

The dataset contains 910 stars: 571 stars from the original HVS survey (Brown et al. 2007c), 331 stars from the new HVS survey (Brown et al. 2009a), and 8 BHB stars from the earliest sample (Brown et al. 2005a). We begin by describing the observables – magnitude, position, velocity – all of which are well-determined. Stellar luminosity is less well-determined and must be inferred from colors and metallicity. We discuss the luminosity estimates and distance determinations in some detail. The observed and derived quantities for each star are listed in Table A1, described in the Appendix.

### 2.1. Photometry

All photometry comes from SDSS Data Release 6 (Adelman-McCarthy et al. 2008). We use uber-calibrated PSF magnitudes, and correct the magnitudes and colors for reddening following Schlegel et al. (1998).

### 2.2. Target Selection

The HVS survey target selection emphasizes outliers in the halo population: we target stars redder in  $(u-g)_0$  than known white dwarfs and bluer in  $(g-r)_0$  than known BHB stars (Brown et al. 2006b). This color cut through the stellar population, illustrated in Figure 1, allows us to detect hypervelocity stars efficiently. The majority of targets, however, are normal halo stars.

Our target selection includes stars with  $17 < g_0 < 19.5$  in the range  $-0.39 < (g-r)_0 < -0.25$  (Brown et al. 2007c) and fainter stars with  $19 < g_0 < 20.5$  over a broader color range  $-0.40 < (g-r)_0 < -0.20$  (Brown et al. 2009a). We also include 8 confirmed BHB

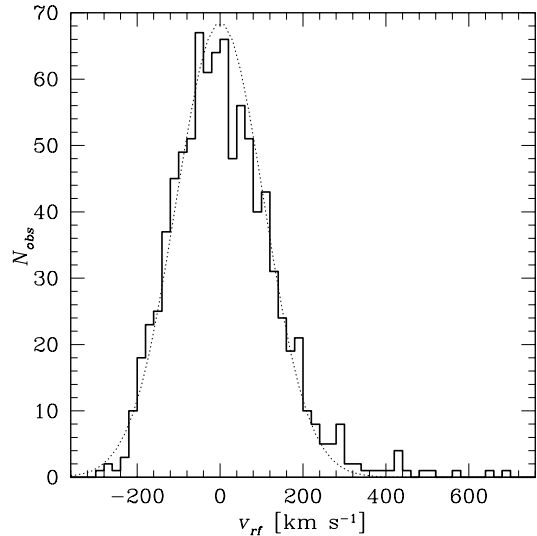


FIG. 2.— Distribution of velocities in the Galactocentric rest frame. The dotted line shows a fiducial Gaussian with zero mean and  $106 \text{ km s}^{-1}$  dispersion. The positive velocity outliers with  $v_{rf} > 400 \text{ km s}^{-1}$  are the unbound HVSs.

stars from Brown et al. (2005a) with  $19.5 < g_0 < 20.25$  and  $-0.3 < (g-r)_0 < -0.1$ . All 910 targets are located in the SDSS DR6 footprint and have an average surface density on the sky of  $0.12 \text{ deg}^{-2}$ .

### 2.3. Radial Velocity

We obtained spectroscopic observations at the 6.5m MMT telescope with the Blue Channel spectrograph. We operated the spectrograph with the  $832 \text{ line mm}^{-1}$  grating in second order, providing wavelength coverage  $3650 \text{ \AA}$  to  $4500 \text{ \AA}$  and a spectral resolution of  $1.2 \text{ \AA}$ . We obtained all observations at the parallactic angle, with a comparison lamp exposure for every survey object.

We processed the data using IRAF<sup>1</sup> in the standard way. We measure radial velocities by cross-correlating the observations with radial velocity standards (Fekel 1999) using the package RVSAO (Kurtz & Mink 1998). The average radial velocity uncertainty of the stars is  $\pm 12 \text{ km s}^{-1}$ .

All velocities discussed here are in the Galactocentric rest frame, indicated  $v_{rf}$ . Given the outer halo location of the stars, we note that the observed radial velocities are almost purely ( $>85\%$ ) radial in the Galactocentric frame. We transform heliocentric velocities ( $v_{helio}$ ) into Galactocentric rest frame velocities assuming a circular velocity of  $220 \text{ km s}^{-1}$  and a solar motion of  $(U, V, W) = (10, 5.2, 7.2) \text{ km s}^{-1}$  (Dehnen & Binney 1998):

$$v_{rf} = v_{helio} + 220 \sin l \cos b + (10 \cos l \cos b + 5.2 \sin l \cos b + 7.2 \sin b). \quad (1)$$

Reid et al. (2009) argue for a larger circular velocity of  $250 \text{ km s}^{-1}$  based on trigonometric parallaxes to star formation regions in the disk. We test using a circular velocity of  $250 \text{ km s}^{-1}$  and find statistically identical

<sup>1</sup> IRAF is distributed by the National Optical Astronomy Observatories, which are operated by the Association of Universities for Research in Astronomy, Inc., under cooperative agreement with the National Science Foundation.

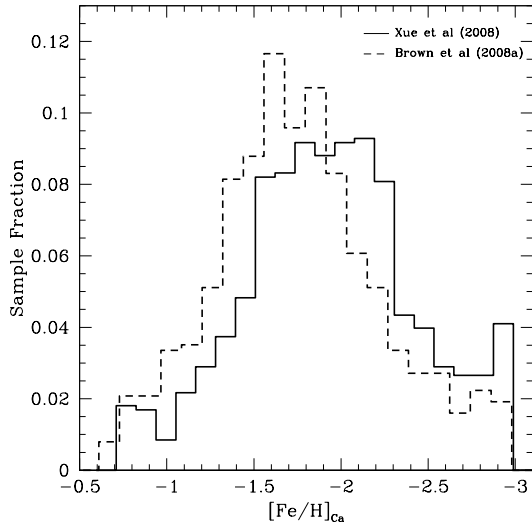


FIG. 3.— Metallicity distribution function of inner halo BHB stars (Brown et al. 2008a) and outer halo BHB stars (Xue et al. 2008) based on Ca II K. The shift towards lower metallicity in the outer halo is expected; the Xue et al. (2008) BHB stars with  $g_0 > 17$  have a mean  $[\text{Fe}/\text{H}]_{\text{Ca}} = -1.9$ .

velocity dispersion profiles. This insensitivity to circular velocity arises because the stars in our high latitude survey have a mean value of  $|\sin l \cos b| = 0.32$ ; changing the Sun’s circular velocity by  $30 \text{ km s}^{-1}$  results in a  $\pm 10 \text{ km s}^{-1}$  change in the stars’ rest frame velocities.  $10 \text{ km s}^{-1}$  is smaller than our measurement error and an order of magnitude smaller than the velocity dispersion of the stars. McMillan & Binney (2009) show that the Reid et al. (2009) data are consistent, at the  $1\text{-}\sigma$  level, with the canonical circular velocity of  $220 \text{ km s}^{-1}$ . Thus we use  $220 \text{ km s}^{-1}$  here.

Figure 2 plots the resulting Galactic rest frame velocity distribution of the 910 halo stars. For reference, we also draw a Gaussian with zero mean and  $106 \text{ km s}^{-1}$  dispersion (dotted line). The observations reveal a significant asymmetry of outliers in the tails of the velocity distribution. There are no stars with  $v_{r,f} < -300 \text{ km s}^{-1}$  but 18 stars with  $v_{r,f} > +300 \text{ km s}^{-1}$  (the HVSSs). We address this issue in Section ??.

#### 2.4. Metallicity

The strongest metal line in our spectra is the  $3933 \text{ \AA}$  Ca II K line. Unfortunately, at the effective temperatures sampled by the survey,  $10,000 \leq T_{\text{eff}} \leq 15,000 \text{ K}$ , the equivalent width of Ca II K is small (Wilhelm et al. 1999a). Thus, Ca II K provides poor leverage on the metallicity of our stars. Metallicity is better determined for redder (cooler) BHB stars, for example the BHB survey of Brown et al. (2008a) and the BHB sample from the SDSS spectroscopic survey (Xue et al. 2008). The metallicity distributions of these two BHB samples are plotted in Figure 3 and are similar in shape. However, the outer halo sample of Xue et al. (2008) is about 0.2 dex more metal-poor than the inner halo sample of Brown et al. (2008a). The mean metallicity of the Xue et al. (2008) BHB stars with  $g_0 > 17$  is  $[\text{Fe}/\text{H}]_{\text{Ca}} = -1.9$ .

To make luminosity estimates, we assume our sur-

vey stars have the metallicity distribution function of Xue et al. (2008). This assumption is reasonable given the very similar sky coverage and penetration into the halo of the two surveys: the stars occupy similar regions of the Milky Way halo. The reddest stars in our sample, where we can estimate metallicity, are metal-poor (Brown et al. 2006b), consistent with the metallicity distribution function of Xue et al. (2008).

#### 2.5. Spectroscopic Identification

Although the stars in our survey have the spectral types of late B- and early A-type stars, their nature is ambiguous. The old stellar population of the halo contains both evolved BHB stars and main sequence blue stragglers. Halo surveys consistently find that  $\sim 50\%$  of A-type stars in the field are blue stragglers (Norris & Hawkins 1991; Kinman et al. 1994; Preston et al. 1994; Wilhelm et al. 1999b; Clewley et al. 2002, 2004; Brown et al. 2003, 2005b, 2008a; Xue et al. 2008). This result is problematic because BHB stars and blue stragglers can have very different luminosities (Figure 1). Spectroscopic measures of surface gravity can discriminate the evolutionary state of the stars (Kinman et al. 1994; Wilhelm et al. 1999a; Clewley et al. 2002, 2004). Unfortunately, surface gravity measures fail for our sample because BHB and main sequence stars have nearly identical surface gravities at the effective temperatures of our stars.

We target stars so blue, however, that we largely exclude the possibility of blue stragglers. A  $\simeq 0.75 M_{\odot}$  star with  $[\text{Fe}/\text{H}] = -1.9$  has a main sequence lifetime of a Hubble time (Girardi et al. 2004). A field blue straggler cannot plausibly have more than twice the mass of a main-sequence turnoff star. In our sample, 36% of the stars are bluer than both  $(g-r)_0 = -0.27$  and  $(u-g)_0 = 0.87$ , the color of a  $1.5 M_{\odot}$  star with  $[\text{Fe}/\text{H}] = -1.9$  (Girardi et al. 2004). Thus the nature of many of the stars is clear: they are hot BHB stars.

Stars bluer than a  $1.5 M_{\odot}$  star are BHB; stars redder than a  $1.5 M_{\odot}$  star are equally likely to be BHB stars or blue stragglers. We base this conclusion on Xue et al. (2008), who observe a BHB fraction of 47% at the red end of our sample. Overall, our sample is 74% BHB stars and 26% blue stragglers.

#### 2.6. Luminosity

We estimate luminosity from stellar evolution tracks. Girardi et al. (2002, 2004) provide main sequence tracks in the SDSS passbands for metallicities ranging from solar to  $[\text{Fe}/\text{H}] = -2.3$ , but do not include the horizontal branch. Dotter et al. (2007, 2008) provide BHB tracks in the SDSS passbands over the same range of metallicities. To simplify the luminosity estimates, we fit low-order polynomials to the tracks as a function of both color and metallicity.

We estimate luminosity two ways, using a star’s  $(u-g)_0$  and  $(g-r)_0$  color. Our final luminosity is the weighted average of the two estimates. We weight by the slope of the observed  $(u-g)_0$  versus  $(g-r)_0$  distribution (Figure 1). This weighting is important because luminosity is most sensitive to  $(u-g)_0$  at the blue end of our sample and to  $(g-r)_0$  at the red end of our sample. The weighting favors luminosities derived from  $(u-g)_0$  for  $(g-r)_0 < -0.24$  and luminosities derived from  $(g-r)_0$

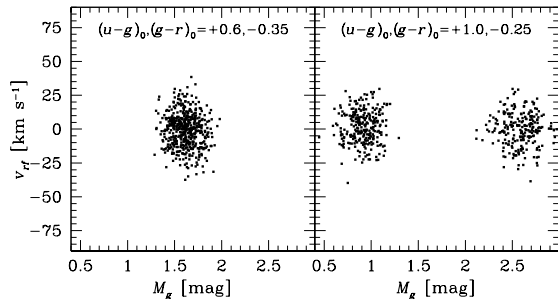


FIG. 4.— Distribution of luminosity  $M_g$  and velocity for fiducial stars in the bluest (left panel) and reddest (right panel) quartiles of our sample. The distributions are obtained by propagating the observed uncertainties of a  $g_0 = 19$  star at the median depth of our survey ( $\sigma_{u-g} = 0.05$ ,  $\sigma_{g-r} = 0.03$ ,  $\sigma_v = 12 \text{ km s}^{-1}$ ) with the Xue et al. (2008) halo metallicity distribution function through stellar evolutionary tracks for main sequence (Girardi et al. 2004) and BHB (Dotter et al. 2008) stars. Blue stars have luminosity precise to 10%, whereas red stars have a bimodal distribution in luminosity (compare with Figure 1).

for  $(g-r)_0 > -0.24$ . Figure 1 shows the resulting lines of constant luminosity for a star with  $[\text{Fe}/\text{H}] = -1.9$  from the Girardi et al. (2004) main sequence tracks (in blue) and from the Dotter et al. (2008) BHB tracks (in red).

The accuracy of the luminosity estimate depends on the accuracy of the stellar evolution models. For example, alpha-enhanced tracks (appropriate for the old stellar halo populations) are systematically bluer than solar-scaled tracks for both main sequence and BHB stars (Lee et al. 2009).

The precision of the luminosity estimate is more robust because we apply the same tracks to all stars. The precision depends on observational uncertainties and is straightforward to quantify. A  $g_0 = 19$  star at the median depth of our survey has uncertainties  $\sigma_{(u-g)} = 0.05$  and  $\sigma_{(g-r)} = 0.03$  in color and  $\sigma_v = 12 \text{ km s}^{-1}$  in velocity. We assume that metallicity is randomly drawn from the Xue et al. (2008) metallicity distribution function (Figure 3). We then propagate these uncertainties through the main sequence and BHB tracks to visualize the resulting distribution of luminosity estimates.

Figure 4 plots the distribution of luminosity and velocity (centered at zero) for two fiducial stars in the bluest quartile (left panel) and the reddest quartile (right panel) of the survey. Stars in the bluest quartile have luminosities precise to 10% because main sequence and BHB stars have essentially identical luminosities at these colors (Figure 1). Stars in the reddest quartile, however, have bimodal luminosity distributions with a factor of 4 spread in luminosity (a factor of 2 in distance). This degeneracy is broken for confirmed BHB stars: 33 of our stars are listed as BHB stars in Xue et al. (2008) and 8 are BHB stars from our earliest sample (Brown et al. 2005a). For these confirmed BHB stars we use only the BHB luminosity to calculate distance.

Three of the stars with  $v_{rf} > +400 \text{ km s}^{-1}$  in this survey are confirmed young main sequence B stars (Fuentes et al. 2006; Bonanos et al. 2008; López-Morales & Bonanos 2008; Przybilla et al. 2008a,b). For the purposes of this paper, however, we treat these HVSS the same as the other stars in our sample: we estimate distances to the HVSS as if they

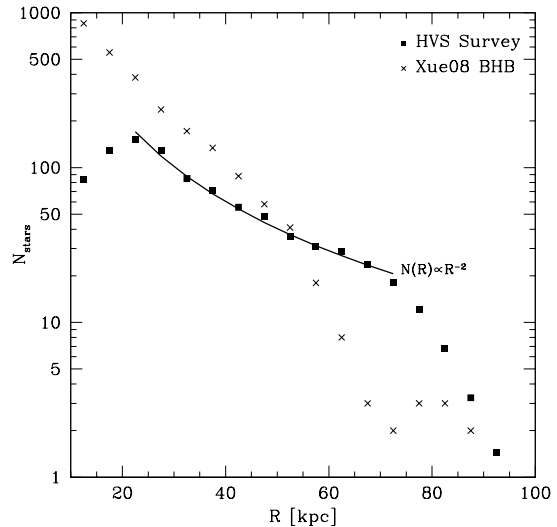


FIG. 5.— Density distribution of the HVS survey stars compared with the Xue et al. (2008) BHB sample. Our survey is complete, but we find an artificially shallow density profile because we observe over a broader color range at large depths  $g_0 > 19$  mag.

were halo BHB stars or metal-poor blue stragglers. We clip the HVSS from the sample when calculating the velocity dispersion in Section ??.

### 2.7. Distance

We calculate distances from the observed apparent magnitudes and estimated luminosities:

$$d = 10^{(g_0 - M_g)/5 - 2} \text{ kpc}, \quad (2)$$

where  $d$  is the heliocentric distance in kpc,  $g_0$  is the apparent magnitude corrected for extinction, and  $M_g$  is the absolute magnitude estimated above. We convert heliocentric distance  $d$  to Galactocentric distance  $R$  with the Sun at  $R = 8 \text{ kpc}$ .

Figure 5 plots the resulting distance distribution of the survey stars compared with the Xue et al. (2008) sample of BHB stars. The Xue et al. (2008) sample contains more than twice as many stars as our sample; however, our sample is deeper and contains twice as many stars with  $R \gtrsim 50 \text{ kpc}$ . Neither sample fairly measures the density profile of the halo. The Xue et al. (2008) sample is incomplete in color, magnitude depth, and spatial coverage. Our sample is complete in all dimensions, but we find an artificially shallow density profile – consistent with  $N(R) \propto R^{-2}$  over the range  $20 < R < 70 \text{ kpc}$  (Figure 5) – because we observe over a broader color range starting at  $g_0 > 19$  mag. A shallow density profile works to our advantage for the velocity dispersion analysis, however, because our stars sample greater distances at a greater relative density.

## 3. HALO VELOCITY DISPERSION PROFILE

Based on the distances and velocities of the sample stars, we calculate the velocity dispersion profile of the Milky Way halo. We use two independent methods to calculate velocity dispersion: a parametric method based on a Milky Way potential model, and a non-parametric method based on the Diaferio & Geller (1997) caustic

technique, originally developed to measure galaxy cluster mass profiles. Using these two methods provides a measure of the systematic error introduced from clipping velocity outliers. We also discuss the systematic error from binary stars and disk stars in our dataset, and we conclude by comparing our velocity dispersion profiles with previous work.

### 3.1. Computational Approach

We use a Monte Carlo approach to model the distance to each star. We assume that photometric and velocity errors are Gaussian distributed, and that the underlying metallicity distribution is that of Xue et al. (2008). We then derive the luminosity for each star by randomly drawing its color and metallicity from the observed distributions and comparing them to the main sequence and BHB tracks (Fig. 1) described above. We sample the distributions 100 times per star. Using a Monte Carlo approach allows us to account for the non-Gaussian distribution of luminosity estimates unique to each star.

The resulting Monte Carlo catalog drawn from the observations produces the “cloud” of velocities and distances shown in Figure 6; the distribution of points reflects the uncertainties in the velocity measurements and the distance estimates of the stars.

We calculate the velocity dispersion profile by grouping stars into 5 or 6 unique bins in distance. The bins have sizes of  $0.33R$ , chosen so that the bins contain at least 70 stars. We require 50 stars to obtain a dispersion with a formal statistical uncertainty of 10%. Bins with smaller occupation have dispersions systematically biased low resulting from small number statistics. Given the distance distribution of our sample, the occupation requirement constrains our velocity dispersion measurements to the region  $15 < R < 75$  kpc. Stars with well-determined luminosities contribute their full weight to a single distance bin; stars with poorly-constrained luminosities contribute less weight distributed over multiple bins.

We use bootstrap re-sampling to calculate the uncertainty in the velocity dispersion measurement. Our procedure is to draw random sets of 910 stars, with replacement, from the Monte Carlo catalog and re-calculate the velocity dispersion. We re-sample 10,000 times; the uncertainty is the standard deviation of the velocity dispersions.

### 3.2. Velocity Dispersion: Potential Model

Our survey was designed to find unbound HVSs. Thus the first step in calculating the velocity dispersion profile is to clip the unbound stars from the sample. Defining an unbound star is difficult, however. The best estimate of the Galactic escape velocity is  $550 \pm 50$  km s<sup>-1</sup> at the solar circle, based on the highest velocity stars in the solar neighborhood (Smith et al. 2007). The escape velocity of the outer halo is more poorly constrained; extrapolating  $v_{esc}(R)$  to large  $R$  requires a potential model.

Here, we use the Kenyon et al. (2008) potential model that is tied to observed Milky Way mass measurements. To establish  $v_{esc}(R)$  in this model, we drop a test particle at rest from  $R = 500$  kpc (i.e., halfway to M31) and calculate its trajectory down to  $R = 0$  kpc. The Kenyon et al. (2008) model predicts  $v_{esc} = 585$  km s<sup>-1</sup> at  $R = 8$  kpc in this definition of escape velocity, in good

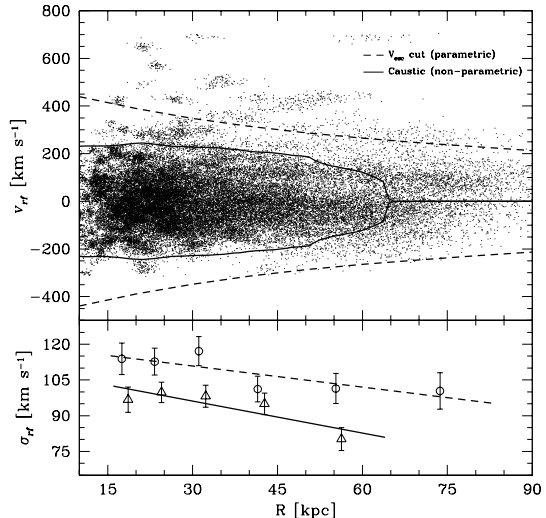


FIG. 6.— Upper panel: Monte Carlo distribution of distance and radial velocity for our sample. We represent each star by 100 random draws from its parent distance and velocity error distribution. We clip velocity outliers using two approaches: a parametric method based on a Milky Way potential model (*dashed line*), and a non-parametric method based on the Diaferio & Geller (1997) caustic technique (*solid line*). Lower panel: binned velocity dispersion profile from the two approaches. Errors are from bootstrap re-sampling. Linear least squares fits show an average  $-0.38 \pm 0.12$  km s<sup>-1</sup> kpc<sup>-1</sup> decline in velocity dispersion over  $15 < R < 75$  kpc.

agreement with the Smith et al. (2007) observation. We fit a low-order polynomial to the calculated velocity as a function of distance and find

$$v_{esc}(R) = -2.30 \times 10^{-4} R^3 + 0.0588 R^2 - 6.62 R + Z \text{ km s}^{-1}, \quad (3)$$

where  $Z = 619$  km s<sup>-1</sup>, valid for  $15 < R < 100$  kpc.

To avoid imposing an arbitrary mass on our velocity dispersion measurement, however, we re-normalize Equation 3 to the observed envelope of negative velocity stars in our sample. Figure 6 shows the  $v_{esc}(R)$  relation that we use, with  $Z = 500$  km s<sup>-1</sup> (Eqn. 3). Our assumption in changing  $Z$  to 500 km s<sup>-1</sup> is that the velocity distribution of halo stars extends up to the escape velocity, and that the most negative velocity stars – the stars falling in from the largest distances – provide the most robust measure of escape velocity in our dataset. Perets et al. (2009) discuss this further in the context of HVSs. We test the effects of our choice of  $v_{esc}(R)$  by using a non-parametric approach to calculate velocity dispersion in the next section. In this section, we calculate the velocity dispersion profile by using the shape of the  $v_{esc}(R)$  relation to provide a physically motivated means of clipping velocity outliers.

We plot the resulting velocity dispersion of stars with velocities less than  $v_{esc}(R)$  for  $Z = 500$  km s<sup>-1</sup> in the lower panel of Figure 6. Our Monte Carlo approach allows outliers that might otherwise be clipped to contribute a weight appropriate to their measurement uncertainties. A linear least squares fit to the velocity dispersion profile finds a declining velocity dispersion,

$$\sigma_v = (-0.30 \pm 0.10) R + (120 \pm 4.6) \text{ km s}^{-1}, \quad (4)$$

valid over  $15 < R < 75$  kpc. A higher-order fit does not significantly improve the residuals. The linear fit

has a standard deviation of  $4.8 \text{ km s}^{-1}$  and a reduced  $\chi^2$  of 0.7. A fixed velocity dispersion, by comparison, has a standard deviation of  $7.6 \text{ km s}^{-1}$  and a reduced  $\chi^2$  of 1.5, poorer than the linear fit but not statistically inconsistent.

### 3.3. Velocity Dispersion: Caustic Method

A non-parametric approach to determining the velocity dispersion profile leads to robust results based on fewer a-priori assumptions. Here we use the caustic technique. Because this technique is new to the stellar halo literature, we begin with an introduction before discussing the mechanics and results. Diaferio (2009) provides a recent review of the technique.

The caustic technique was originally developed to measure galaxy cluster mass profiles (Diaferio & Geller 1997; Diaferio 1999). Caustics are essentially escape velocity curves. The caustic technique is based on the distribution of objects in phase space: the line-of-sight velocity  $v$  vs. projected distance  $r$  from the cluster center. In this plane, cluster members distribute in a characteristic trumpet shape with upper and lower borders indicating the escape velocity from the system. The amplitude  $\mathcal{A}(r)$  of this distribution, which decreases with  $r$ , is a direct measure of the escape velocity from the system, independent of its dynamical state. The caustic technique only assumes that the spatial distribution of tracers is spherically symmetric.

The caustic technique can be applied to any self-gravitating system. The technique is non-parametric and does not require that the tracers of the potential be in virial equilibrium. It is an effective tool for identifying bound members of the system defined by the upper and lower caustics (sharp declines in phase space density of tracers). For example, Serra et al. (2009) apply the caustic technique to five dwarf spheroidals of the Milky Way.

Applying the caustic technique to the halo star sample requires a slight modification of the procedure used for galaxy clusters. Traditionally, the technique arranges sample objects in a binary tree according to their pairwise projected binding energies (Diaferio 1999). By walking along the main branch of the tree, the technique determines the velocity dispersion which locates the caustic in the velocity diagram. This step does not apply to the Milky Way halo; the stars are not obviously clustered on the sky and the estimate of the pairwise binding energy is inappropriate. Thus we apply the technique directly to the phase space diagram shown in Figure 6.

The caustics are the curves satisfying the equation  $f_q(r, v) = \kappa$ , where  $f_q(r, v)$  is the distribution in the phase space diagram, and  $\kappa$  is the root of the equation  $\langle v_{\text{esc}}^2 \rangle_{\kappa, R} = 4\sigma^2$ . The function

$$\langle v_{\text{esc}}^2 \rangle_{\kappa, R} = \int_0^R \mathcal{A}_\kappa^2(r) \varphi(r) dr / \int_0^R \varphi(r) dr \quad (5)$$

is the mean caustic amplitude within  $R$ ,  $\varphi(r) = \int f_q(r, v) dv$ .  $R$  is not a free parameter in the standard application of the technique, but here we chose  $R = 30 \text{ kpc}$ . Our results are totally insensitive to this parameter: varying  $R$  in the range 20-100 kpc varies the final number of the halo members by at most five and does not change the velocity dispersion profile.

We use an iterative approach to estimate the velocity dispersion profile. First we compute the velocity dis-

persion of the total sample and locate the caustics that enable some interloper removal. We then compute a new velocity dispersion with the member stars, locate new caustics and remove further interlopers. We proceed until no star is identified as an interloper. This procedure requires only four steps and on average yields 838 (of 910) final halo members and an overall velocity dispersion of  $99 \text{ km s}^{-1}$ . The final set of caustics are drawn with the solid line in the upper panel of Figure 6.

The open triangles in the lower panel of Figure 6 show the caustic velocity dispersion profile. It is visually apparent that the caustic technique measures the velocity dispersion from the well-sampled core of the velocity distribution. This approach results in a reliable velocity dispersion profile, but yields a velocity dispersion that is systematically 10% smaller than found by our parametric  $v_{\text{esc}}(R)$  method. We conclude that clipping velocity outliers with the caustic technique changes the observed amplitude, but not the observed slope, of the velocity dispersion profile.

A linear least squares fit to the caustic velocity dispersion profile finds a declining velocity dispersion,

$$\sigma_v = (-0.45 \pm 0.16)R + (110 \pm 6.0) \text{ km s}^{-1}, \quad (6)$$

valid over  $16 < R < 64 \text{ kpc}$ . The linear fit has a standard deviation of  $4.8 \text{ km s}^{-1}$  and a reduced  $\chi^2$  of 1.0. A fixed velocity dispersion, by comparison, has a standard deviation of  $7.9 \text{ km s}^{-1}$  and a reduced  $\chi^2$  of 2.8. In this case, a constant velocity dispersion is a significantly poorer fit to the data.

### 3.4. Possible Systematics

There are at least two contaminants that may systematically affect our velocity dispersion profile: binary stars, which increase the velocity dispersion, and disk stars (i.e. white dwarfs), which decrease the velocity dispersion. We investigate how these contaminants may alter the observed velocity dispersion profile.

Binary stars are unlikely to change the velocity dispersion profile. Both BHB stars and  $1.5 M_\odot$  blue stragglers have stellar radii around  $2.5 R_\odot$ . Equal mass pairs of such stars must have semimajor axes of at least  $6.5 R_\odot$  to avoid Roche lobe overflow. Thus the most compact possible binary system has velocity semi-amplitude of  $100 \text{ km s}^{-1}$ . Assuming that half of the targets are binaries with a log-normal distribution of semimajor axes, we expect 30 binaries in our dataset with  $v \sin i > 50 \text{ km s}^{-1}$ . This estimate is generous given that BHB stars have recently evolved through the red giant phase and are thus unlikely to have close companions. In any case, binaries will be observed at a random orbital phase and binned with 70-200 other stars to compute a velocity dispersion. We propagate our simulated distribution of  $v \sin i$ 's through our Monte Carlo catalog and find a negligible change in the velocity dispersion profile; the uncertainty in the velocity dispersion slope remains 30%.

Disk stars pose a greater threat to the velocity dispersion profile. Disk stars have a systematically lower velocity dispersion than halo stars and may also have a non-zero mean velocity because of the longitude dependence of the Sun's circular velocity correction. The SDSS imaging survey from which we draw our candidates does not uniformly survey the sky across all longitudes.

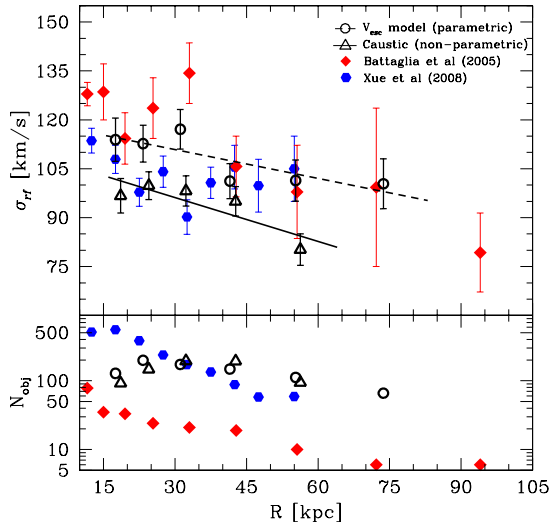


FIG. 7.— Milky Way velocity dispersion profile (upper panel): this paper (*open symbols*), Battaglia et al. (2005) (*red diamonds*), and Xue et al. (2008) (*blue hexagons*). Number distribution with radius (lower panel, same symbols).

Our greatest concern is white dwarfs, which are intrinsically faint and overwhelmingly appear at faint magnitudes in our survey. Inserting white dwarfs into our halo sample thus reduces the velocity dispersion observed at large distances. Observationally, 15% of our survey targets are white dwarfs, mostly found at low latitudes. If we insert a 1% white dwarf contamination into our Monte Carlo catalog, the resulting velocity dispersion profile steepens by 10%. Fortunately, white dwarfs are readily identified by their broad Balmer lines (see Kilic et al. 2007a). Visual inspection of our spectra reveals no white dwarf contaminants.

Binaries also have observational constraints. We obtained repeat observations for every star with  $|v_{rf}| > 300 \text{ km s}^{-1}$  and found only one star, a star near  $-300 \text{ km s}^{-1}$ , to exhibit radial velocity variation. We thus excluded this star from the halo sample. We conclude that binaries and white dwarfs are unlikely to significantly influence the velocity dispersion profile measured from our halo star sample.

### 3.5. Comparison with Previous Results

There are few measurements of the Milky Way velocity dispersion profile at large  $R$ . The most comparable measurements are Battaglia et al. (2005) and Xue et al. (2008). Battaglia et al. (2005) measure the velocity dispersion profile based on a sample of 9 satellite galaxies, 44 globular clusters, 58 red giants, and 130 BHB stars that span  $10 < R < 140 \text{ kpc}$ . Xue et al. (2008) measure the velocity dispersion profile based on a sample of 2401 BHB stars that span  $5 < R < 60 \text{ kpc}$ . With the exception of a handful of shared BHB stars, the samples are independent of one another.

Figure 7 compares the velocity dispersion profile and radial number distribution of our sample with those of Battaglia et al. (2005) and Xue et al. (2008). Beyond  $R > 50 \text{ kpc}$ , our sample contains a factor of 8 more stars than Battaglia et al. (2005) and a factor of 2 more stars

than Xue et al. (2008). Remarkably, the velocity dispersions measured by the three samples are consistent at the  $1.5\text{-}\sigma$  level. The three samples also observe a statistically similar decline in velocity dispersion with distance. The major difference between the samples is the significance of the observed decline in velocity dispersion with distance.

A linear least squares fit to the Xue et al. (2008) data gives a  $-0.15 \pm 0.14 \text{ km s}^{-1} \text{ kpc}^{-1}$  decline in velocity dispersion over  $10 < R < 60 \text{ kpc}$ . The linear fit has a standard deviation of  $6.3 \text{ km s}^{-1}$  and a reduced  $\chi^2$  of 1.5. A fixed velocity dispersion has a very similar standard deviation of  $6.4 \text{ km s}^{-1}$  and reduced  $\chi^2$  of 1.9. Thus the Xue et al. (2008) measurements cannot formally discriminate between a constant velocity dispersion and a declining velocity dispersion.

The Battaglia et al. (2005) data, on the other hand, exhibit a steeper  $-0.58 \pm 0.11 \text{ km s}^{-1} \text{ kpc}^{-1}$  decline in velocity dispersion over  $10 < R < 100 \text{ kpc}$ . We exclude their last bin because it contains only 3 objects. The linear fit has a standard deviation of  $8.6 \text{ km s}^{-1}$  and a reduced  $\chi^2$  of 0.85.

The weighted average of all the samples yields a  $-0.38 \pm 0.12 \text{ km s}^{-1} \text{ kpc}^{-1}$  decline in velocity dispersion over  $10 < R < 100 \text{ kpc}$ . We obtain the same result if we average only our own two velocity dispersion measurements. The Milky Way velocity dispersion profile is not linear, of course, but three independent sets of observations are in statistical agreement: the Milky Way radial velocity dispersion drops from  $\sigma \simeq 110 \text{ km s}^{-1}$  at  $R = 15 \text{ kpc}$  to  $\sigma \simeq 85 \text{ km s}^{-1}$  at  $R = 80 \text{ kpc}$ .

## 4. CONCLUSIONS

The mass and mass distribution of the Milky Way are fundamental parameters because they link directly to theoretical models. We use a spectroscopic sample of 910 halo stars derived from our HVS survey to measure the velocity dispersion profile of the Milky Way. The stars are 74% BHB stars and 26% blue stragglers. We estimate luminosities using stellar evolution tracks for metal poor main sequence stars and BHB stars. Because of the non-Gaussian distribution of luminosity estimates, we use a Monte Carlo approach to calculate velocity dispersion and its uncertainty.

We calculate the velocity dispersion profile in two ways: a parametric method based on a  $v_{esc}(R)$  model, and a non-parametric method based on the caustic technique originally developed to measure galaxy cluster mass profiles. Comparing the two methods provides a measure of the systematic uncertainty arising from the clipping of outliers in velocity. The velocity dispersion from the caustic method is 10% smaller than the  $v_{esc}(R)$  method, but both methods identify a similar decline in velocity dispersion with distance:  $-0.38 \pm 0.12 \text{ km s}^{-1} \text{ kpc}^{-1}$ , valid for  $15 < R < 75 \text{ kpc}$ .

Our sample contains a factor of 8 more stars than Battaglia et al. (2005) and a factor of 2 more stars than Xue et al. (2008) at  $R > 50 \text{ kpc}$ . The velocity dispersion profiles observed by these independent datasets are consistent at the  $1.5\text{-}\sigma$  level, and have an average velocity dispersion slope identical to our result. Remarkably, no matter what tracers are used, observers find the same halo velocity dispersion profile.

The velocity dispersion profile is a basis for measuring

TABLE A1  
DATA TABLE

RA hrs (1)	Dec deg (2)	$g_0$ mag (3)	$\sigma_g$ mag (4)	$(u-g)_0$ mag (5)	$\sigma_{(u-g)}$ mag (6)	$(g-r)_0$ mag (7)	$\sigma_{(g-r)}$ mag (8)	$v_{helio}$ km s <sup>-1</sup> (9)	$\sigma_v$ km s <sup>-1</sup> (10)	$l$ deg (11)	$b$ deg (12)	$v_{rf}$ km s <sup>-1</sup> (13)	$M_{g,BHB}$ mag (14)	$\sigma_B$ mag (15)
0:02:05.713	31:18:50.23	20.434	0.026	0.778	0.095	-0.277	0.040	-209.3	14.0	110.717	-30.385	-34.3	1.17	0.0
0:02:33.817	-9:57:06.85	18.434	0.021	0.753	0.040	-0.328	0.040	-87.7	9.7	86.763	-69.316	-14.8	1.31	0.0
0:04:36.491	-9:57:19.48	19.834	0.018	0.922	0.103	-0.167	0.032	-172.6	35.0	87.977	-69.584	-100.7	0.69	0.0
0:05:28.141	-11:00:10.07	19.141	0.042	1.007	0.081	-0.275	0.047	-115.9	10.9	86.890	-70.586	-47.8	0.94	0.0
0:07:52.013	-9:19:54.32	17.302	0.017	1.016	0.036	-0.276	0.039	-114.5	9.9	90.855	-69.443	-42.2	0.91	0.0
0:12:26.890	-10:47:54.56	18.898	0.025	1.006	0.064	-0.321	0.038	-128.2	10.5	91.741	-71.269	-62.8	0.94	0.0
0:23:53.294	-1:04:46.40	18.199	0.016	0.749	0.042	-0.255	0.025	19.7	9.8	107.552	-63.125	109.0	1.15	0.0
0:29:31.158	15:39:40.20	19.069	0.024	1.057	0.069	-0.270	0.038	22.3	35.0	115.201	-46.881	153.4	0.88	0.0
0:36:40.570	-11:11:25.02	17.421	0.018	0.778	0.028	-0.304	0.031	32.5	9.8	109.940	-73.689	84.1	1.26	0.0
0:39:06.749	24:09:05.62	19.348	0.018	0.948	0.081	-0.255	0.030	-130.0	35.0	119.332	-38.634	15.0	0.94	0.0

NOTE. — Table A1 is presented in its entirety in the electronic edition of the *Astrophysical Journal*. A portion is shown here for guidance and content.

the total mass and mass distribution of the Milky Way halo. A companion paper by Gnedin et al. (in preparation) presents the theoretical calculations that turn the observed velocity dispersion profile into a mass determination of the Milky Way.

For further progress in measuring the Milky Way velocity dispersion profile, it is essential to identify tracers at distances  $R > 50$  kpc. It is difficult to find  $R > 50$  kpc tracers because of the steep decline in the density of the stellar halo. It is also very difficult for proper motion surveys to measure tracers at  $R > 50$  kpc distances. On-going spectroscopic radial velocity surveys, such as the SDSS-3 survey and our own HVS survey, promise to better trace the Milky Way in coming years.

We thank M. Alegria, J. McAfee, and A. Milone for their assistance with observations obtained at the MMT Observatory, a joint facility of the Smithsonian Institution and the University of Arizona. We also thank the referee and Oleg Gnedin for helpful comments that improved this paper. This project makes use of data products from the Sloan Digital Sky Survey, which is managed by the Astrophysical Research Consortium for the Participating Institutions. This research makes use of NASA's Astrophysics Data System Bibliographic Services. AD gratefully acknowledges partial support from INFN grant PD51. This work was supported by the Smithsonian Institution.

*Facilities:* MMT (Blue Channel Spectrograph)

## APPENDIX

### DATA TABLE

Table A1 presents the 910 stars used here. We provide the observed positions, magnitudes, and velocities plus our derived luminosities, distances, and BHB likelihood. The table columns are: (1) RA (J2000), (2) Dec (J2000), (3) dereddened SDSS  $g_0$  magnitude, (4) magnitude error, (5) dereddened SDSS  $(u-g)_0$  color, (6)  $(u-g)_0$  error, (7) dereddened SDSS  $(g-r)_0$  color, (8)  $(g-r)_0$  error, (9) heliocentric radial velocity  $v_{helio}$ , (10) velocity error, (11) Galactic longitude  $l$ , (12) Galactic latitude  $b$ , (13) Galactic rest frame velocity  $v_{rf}$ , as defined in Equation 1, (14) BHB absolute magnitude  $M_{g,BHB}$  derived from Dotter et al. (2008) for  $[\text{Fe}/\text{H}]=-1.9$ , (15) magnitude error, (16) BHB Galactocentric distance  $R_{BHB}$ , (17) blue straggler absolute magnitude  $M_{g,BS}$  derived from Girardi et al. (2004) for  $[\text{Fe}/\text{H}]=-1.9$ , (18) magnitude error, (19) blue straggler Galactocentric distance  $R_{BS}$ , and (20) the star's likelihood of being BHB,  $0 < f_{BHB} < 1$ , based on stellar colors and spectra. Table A1 is available in its entirety in machine-readable form in the online journal. A portion of the table is shown here for guidance regarding its form and content.



## REFERENCES

- Abadi, M. G., Navarro, J. F., & Steinmetz, M. 2009, *ApJ*, 691, L63
- Adelman-McCarthy, J. K. et al. 2008, *ApJS*, 175, 297
- Battaglia, G., Helmi, A., Morrison, H., Harding, P., Olszewski, E. W., Mateo, M., Freeman, K. C., Norris, J., & Shectman, S. A. 2005, *MNRAS*, 364, 433
- Bonanos, A. Z., López-Morales, M., Hunter, I., & Ryans, R. S. I. 2008, *ApJ*, 675, L77
- Brown, W. R., Allende Prieto, C., Beers, T. C., Wilhelm, R., Geller, M. J., Kenyon, S. J., & Kurtz, M. J. 2003, *AJ*, 126, 1362
- Brown, W. R., Beers, T. C., Wilhelm, R., Allende Prieto, C., Geller, M. J., Kenyon, S. J., & Kurtz, M. J. 2008a, *AJ*, 135, 564
- Brown, W. R., Geller, M. J., & Kenyon, S. J. 2009a, *ApJ*, 690, 1639
- Brown, W. R., Geller, M. J., Kenyon, S. J., & Bromley, B. C. 2009b, *ApJ*, 690, L69
- Brown, W. R., Geller, M. J., Kenyon, S. J., & Kurtz, M. J. 2005a, *ApJ*, 622, L33
- . 2006a, *ApJ*, 640, L35
- . 2006b, *ApJ*, 647, 303
- . 2007a, *ApJ*, 666, 231
- Brown, W. R., Geller, M. J., Kenyon, S. J., Kurtz, M. J., Allende Prieto, C., Beers, T. C., & Wilhelm, R. 2005b, *AJ*, 130, 1097
- Brown, W. R., Geller, M. J., Kenyon, S. J., Kurtz, M. J., & Bromley, B. C. 2007b, *ApJ*, 660, 311
- . 2007c, *ApJ*, 671, 1708
- Brown, W. R., Kewley, L. J., & Geller, M. J. 2008b, *AJ*, 135, 92
- Clewley, L., Warren, S. J., Hewett, P. C., Norris, J. E., & Evans, N. W. 2004, *MNRAS*, 352, 285
- Clewley, L., Warren, S. J., Hewett, P. C., Norris, J. E., Peterson, R. C., & Evans, N. W. 2002, *MNRAS*, 337, 87
- Dehnen, W. & Binney, J. J. 1998, *MNRAS*, 298, 387
- Diaferio, A. 1999, *MNRAS*, 309, 610
- . 2009, arXiv:0901.0868
- Diaferio, A. & Geller, M. J. 1997, *ApJ*, 481, 633
- Dotter, A., Chaboyer, B., Jevremović, D., Baron, E., Ferguson, J. W., Sarajedini, A., & Anderson, J. 2007, *AJ*, 134, 376
- Dotter, A., Chaboyer, B., Jevremović, D., Kostov, V., Baron, E., & Ferguson, J. W. 2008, *ApJS*, 178, 89
- Fekel, F. C. 1999, in *ASP Conf. Ser. 185: IAU Colloq. 170: Precise Stellar Radial Velocities*, ed. J. B. Hearnshaw & C. D. Scarfe (San Francisco: ASP), 378
- Fuentes, C. I., Stanek, K. Z., Gaudi, B. S., McLeod, B. A., Bogdanov, S., Hartman, J. D., Hickox, R. C., & Holman, M. J. 2006, *ApJ*, 636, L37
- Girardi, L., Bertelli, G., Bressan, A., Chiosi, C., Groenewegen, M. A. T., Marigo, P., Salasnich, B., & Weiss, A. 2002, *A&A*, 391, 195
- Girardi, L., Grebel, E. K., Odenkirchen, M., & Chiosi, C. 2004, *A&A*, 422, 205
- Hernandez, X., Mendoza, S., Suarez, T., & Bernal, T. 2009, arXiv:0904.1434
- Kalberla, P. M. W. & Dedes, L. 2008, *A&A*, 487, 951
- Kenyon, S. J., Bromley, B. C., Geller, M. J., & Brown, W. R. 2008, *ApJ*, 680, 312
- Kewley, L. J., Brown, W. R., Geller, M. J., Kenyon, S. J., & Kurtz, M. J. 2007, *AJ*, 133, 882
- Kilic, M., Allende Prieto, C., Brown, W. R., & Koester, D. 2007a, *ApJ*, 660, 1451
- Kilic, M., Brown, W. R., Allende Prieto, C., Pinsonneault, M., & Kenyon, S. 2007b, *ApJ*, 664, 1088
- Kinman, T. D., Suntzeff, N. B., & Kraft, R. P. 1994, *AJ*, 108, 1722
- Kochanek, C. S. 1996, *ApJ*, 457, 228
- Kulesa, A. S. & Lynden-Bell, D. 1992, *MNRAS*, 255, 105
- Kurtz, M. J. & Mink, D. J. 1998, *PASP*, 110, 934
- Lee, H.-c., Worthey, G., & Dotter, A. 2009, *AJ*, arXiv:0905.1947
- Li, Y.-S. & White, S. D. M. 2008, *MNRAS*, 384, 1459
- Little, B. & Tremaine, S. 1987, *ApJ*, 320, 493
- López-Morales, M. & Bonanos, A. Z. 2008, *ApJ*, 685, L47
- McMillan, P. J. & Binney, J. J. 2009, *MNRAS*, submitted, arXiv:0907.4685
- Navarro, J. F., Frenk, C. S., & White, S. D. M. 1997, *ApJ*, 490, 493
- Norris, J. E. & Hawkins, M. R. S. 1991, *ApJ*, 380, 104
- Perets, H. B., Wu, X., Zhao, H. S., Famaey, B., Gentile, G., & Alexander, T. 2009, *ApJ*, 697, 2096
- Preston, G. W., Beers, T. C., & Shectman, S. A. 1994, *AJ*, 108, 538
- Przybilla, N., Nieva, M. F., Heber, U., Firnstein, M., Butler, K., Napiwotzki, R., & Edelmann, H. 2008a, *A&A*, 480, L37
- Przybilla, N., Nieva, M. F., Tillich, A., Heber, U., Butler, K., & Brown, W. R. 2008b, *A&A*, 488, L51
- Reid, M. J. et al. 2009, *ApJ*, 700, 137
- Sakamoto, T., Chiba, M., & Beers, T. C. 2003, *A&A*, 397, 899
- Schlegel, D. J., Finkbeiner, D. P., & Davis, M. 1998, *ApJ*, 500, 525
- Serra, A. L., Angus, G. W., & Diaferio, A. 2009, submitted, arXiv:0907.3691
- Smith, M. C. et al. 2007, *MNRAS*, 379, 755
- Sommer-Larsen, J., Beers, T. C., Flynn, C., Wilhelm, R., & Christensen, P. R. 1997, *ApJ*, 481, 775
- Wilhelm, R., Beers, T. C., & Gray, R. O. 1999a, *AJ*, 117, 2308
- Wilhelm, R., Beers, T. C., Sommer-Larsen, J., Pier, J. R., Layden, A. C., Flynn, C., Rossi, S., & Christensen, P. R. 1999b, *AJ*, 117, 2329
- Wilkinson, M. I. & Evans, N. W. 1999, *MNRAS*, 310, 645
- Xue, X. et al. 2008, *ApJ*, 684, 1143
- Zaritsky, D., Olszewski, E. W., Schommer, R. A., Peterson, R. C., & Aaronson, M. 1989, *ApJ*, 345, 759